A two-photon ratiometric fluorescence probe for Cupric Ions in Live Cells and Tissues

Anwei Zhu, Changqin Ding & Yang Tian

Department of Chemistry, Tongji University, Siping Road 1239, Shanghai 200092, China.

Development of sensitive and selective probes for cupric ions (Cu^{2+}) at cell and tissue level is a challenging work for progress in understanding the biological effects of Cu^{2+}. Here, we report a ratiometric two-photon probe for Cu^{2+} based on the organic-inorganic hybrids of graphene quantum dots (GQDs) and Nile Blue dye. Meanwhile, Cu-free derivative of copper-zinc superoxide dismutase (SOD) – E_2Zn_2SOD is designed as the unique receptor for Cu^{2+} and conjugated on the surface of GQDs. This probe shows a blue-to-yellow color change in repose to Cu^{2+}, good selectivity, low cytotoxicity, long-term photostability, and insensitivity to pH over the biologically relevant pH range. The developed probe allows the direct visualization of Cu^{2+} levels in live cells as well as in deep-tissues at 90–180 μm depth through the use of two-photon microscopy. Furthermore, the effect of ascorbic acid is also evaluated on intracellular Cu^{2+} binding to E_2Zn_2SOD by this probe.

Copper (Cu) is an essential trace element which ranks the third in abundance in the human body, and plays a pivotal role in many metabolic processes[1]. The ability of Cu to cycle between stable oxidized Cu^{2+} and unstable reduced Cu^+ states is used by cuproenzymes involved in redox reactions, e.g., Cu, Zn-superoxide dismutase and cytochrome oxidase[2]. However, the $Cu^{2+/+}$ redox can in certain circumstances result in the generation of reactive oxygen species, which if not detoxified efficiently, would damage susceptible cellular components[3,4]. Alterations in the cellular copper homeostasis may also cause cell death and neurodegenerative diseases including Alzheimer's disease, Wilson's disease, Parkinson's disease, and so on[5–7]. Because the bulk of intracellular copper is believed to be present in its monovalent oxidation state (Cu^+), more attention has been paid on the development of fluorescence probes for imaging and biosensing of Cu^+ [8–10]. Actually, the cupric state (Cu^{2+}) is found most often in biological system[11]. It is as important as Cu^+ in cellular copper homeostasis and redox cycling processes of Cu^{12}.

Up to now, a few efficient fluorescent sensors for Cu^{2+}-selective detection have been reported[13–20]. We have also developed a ratiometric strategy for intracellular sensing and imaging of Cu^{2+}, with high sensitivity and accuracy[18,19]. However, most of these probes have been evaluated using one-photon microscopy and require relatively short excitation wavelengths, limiting their use in deep-tissue imaging because of the shallow penetration depth (<80 μm). To determine Cu^{2+} deep inside living tissues, it is crucial to use two-photon microscopy (TPM), a new technique that utilizes near-IR two-photon excitation[21–30]. TPM offers several advantages such as larger imaging depth (>500 μm), minimized autofluorescence background, and less photodamage associated with the use of near infrared excitation. In the past decades, organic dyes and semiconductor quantum dots (QDs) are widely studied two-photon probes[21,25,31,32]. But the rapid photobleaching effect and limited two-photon absorption cross-section of organic dyes hamper the imaging depth. The potential hazard of heavy metals in semiconductor QDs causes concern for in vivo bioimaging, despite of their strong two-photon fluorescence. Recently, graphene quantum dots (GQDs) have emerged as promising fluorescent materials with their good biocompatibility and photostability[33–37]. Two-photon imaging using the GQDs has also been reported for cell labeling[38]. However, no research about applications of GQDs as two-photon probes to sense biological activities or molecules has been reported so far.

In this article, we report a GQDs-based two-photon ratiometric probe for imaging and sensing of Cu^{2+} in live cells and tissues with high selectivity and sensitivity. Three new strategies were developed in the present work. First, as shown in Fig. 1, the GQDs emitting blue fluorescence is hybridized with Nile Blue organic dye emitting red fluorescence as dual-emission fluorophore (GQD@Nile nanohybrid), in which Nile Blue is inert to Cu^{2+} and only serves as reference signal for providing built-in correction to avoid environmental effects. Next, Cu-free
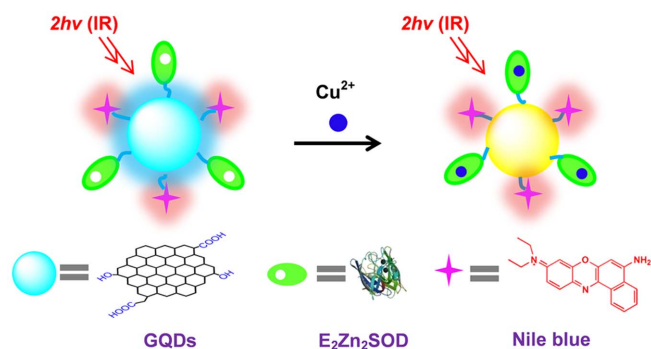
Figure 1 | The working principle of the two-photon ratiometric imaging and sensing of Cu²⁺.

derivative of bovine liver copper-zinc superoxide dismutase (SOD) – E_2Zn_2SOD (E designates an empty site) is employed as the unique receptor specific for Cu^{2+} because E_2Zn_2SOD can interact with Cu^{2+} with high specificity to reconstitute SOD[39–41]. Then, the specific E_2Zn_2SOD is conjugated with the GQD@Nile to form the GQD@Nile-E_2Zn_2SOD fluorescent probe. The organic-inorganic hybrided probe shows dual emission bands centered at ∼465 and ∼675 nm, respectively, upon two-photon (800 nm) excitation. The GQDs functionalized with E_2Zn_2SOD can selectively recognize Cu^{2+}, leading to blue fluorescence quenching, whereas the red fluorescence of Nile Blue stays constant. Consequently, variations of the two fluorescence intensities display clear color changes from blue to yellow upon addition of Cu^{2+}, resulting in a ratiometric two-photon fluorescent sensor for Cu^{2+}. This probe also demonstrates high selectivity for Cu^{2+} over other metal ions and amino acids. Finally, the remarkable analytical performance of the present probe including high sensitivity and selectivity, as well as the fascinating properties of GQDs such as excellent aqueous stability, good biocompatibility, and long-term photostability, enables the imaging and sensing of Cu^{2+} in live cells and tissues at depths of 90–180 μm by TPM. To the best of our knowledge, this is the first report for development of a two-photon ratiometric fluorescence probe suitable for detection of Cu^{2+} in live cells and tissues.

Results

GQDs were prepared by tailoring the carbonization degree of citric acid according to the previous report[42]. The as-made GQDs are mono-dispersed with an average size of ∼10 nm (Fig. 2a) and a topographic height of ∼2 nm (Fig. 2b)[35,36]. A broad diffraction peak corresponding to (002) planes of graphite was observed at around 25° in the X-ray diffraction (XRD) pattern (Fig. 2a) of GQDs, suggesting that carbonizing citric acid would produce graphite structures[43–45]. The Fourier transform infrared (FT-IR) spectrum of the GQDs was given in Fig. 2c (curve I). Five peaks located at 3447 (v_{O-H}), 1685 ($v_{C=O}$), 1588 (v_{COO-}), 1386 (v_{COO-}), and 1119 cm⁻¹ (v_{C-OH}) were observed. The presence of these hydrophilic groups including –COOH and/or –OH imparts GQDs water-solubility. Then, the two-photon ratiometric probe was developed by conjugating GQDs with amino-containing Nile Blue chloride and
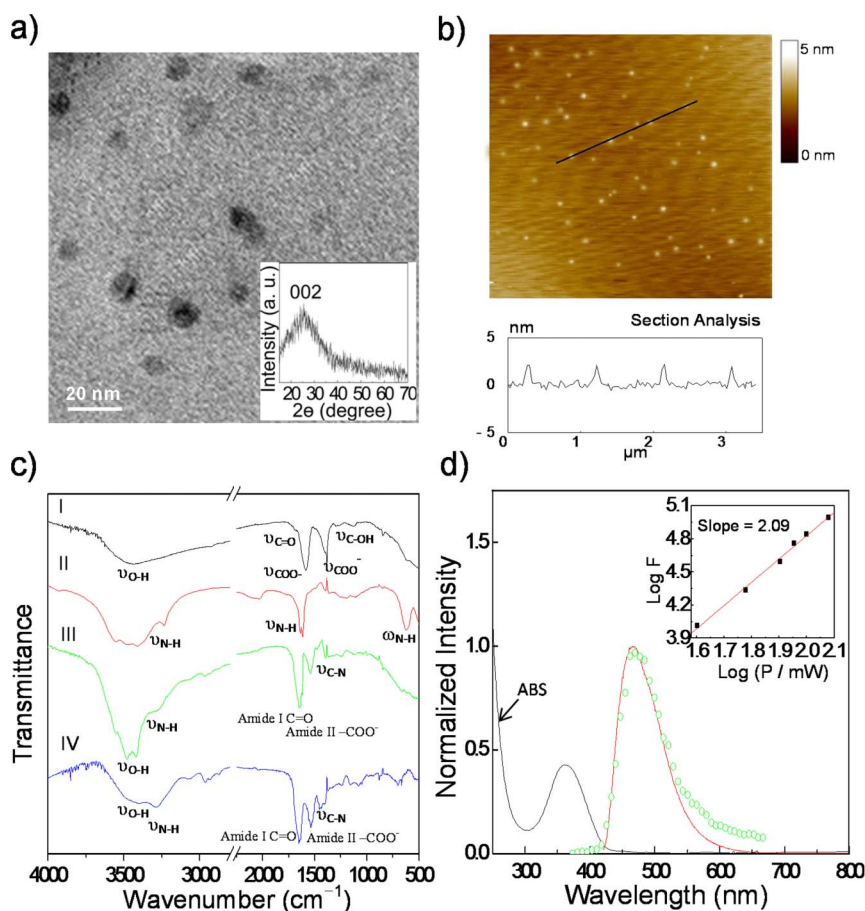

Figure 2 | (a) TEM image of GQDs. Inset: XRD pattern for the GQDs. (b) AFM topography image of GQDs on mica substrates with the height profiles along the line in the image. (c) FT-IR spectra of (I) GQDs, (II) Nile blue, (III) E_2Zn_2SOD and (IV) GQD@Nile-E_2Zn_2SOD. (d) UV-Vis absorption, one-photon (solid line, 400 nm excitation) and two-photon (circle, 800 nm excitation) luminescence spectra of the GQDs. Inset: the quadratic relationship of the observed two-photon luminescent intensity of the GQDs with the excitation laser power at 800 nm.

E_2Zn_2SOD in an activation reaction with 1-ethyl-3-(3-dimethylaminopropyl) carbodiimide hydrochloride (EDC) and N-Hydroxysuccinimide (NHS). The modification of Nile Blue dye and E_2Zn_2SOD onto the surface of GQDs was confirmed by FT-IR and X-ray photoelectron spectroscopy (XPS). Four peaks were clearly observed at 3292 (ν_{N-H}), 1645 (Amide I C=O), 1539 (Amide II -COO$^-$), and 1450 cm^{-1} (ν_{C-N}) in the FT-IR spectra of GQD@Nile-E_2Zn_2SOD (Fig. 2c, curve IV), which suggests the successful attachment of Nile Blue and E_2Zn_2SOD onto the surface of GQDs. In addition, the conjugated process was also tracked by XPS. As shown in Fig. S1, after the conjugation of Nile blue onto the GQDs surface, two new N_{1s} peaks were found at 399.9 eV and 401.7 eV, which are attributed to amide nitrogen and quaternary ammonium nitrogen, respectively (curve II)[46]. The observation of S_{2p} peak (Fig. S1) of thiol group or disulfide at 163.0 eV is evident the exact modification of E_2Zn_2SOD on the GQD@Nile surface, because this peak cannot be obtained at the surfaces of bare GQDs or GQD@Nile.

Upon both one-photon and two-photon excitation, the aqueous solution of GQDs was found to be strongly emissive in the visible and shows an emission maximum at 465 nm. As shown in the inset of Fig. 2d, the quadratic relationship between the excitation laser power and the luminescence intensity is obvious, thus confirming that the excitation with two near-infrared photons was indeed responsible for the observed visible luminescence of GQDs. Using quinine sulfate as a standard, the fluorescence quantum yield (Φ_F) of GQDs was calculated to be $8.2 \pm 1.0\%$[47]. The excitation-independent emission of the GQDs (data not shown) and the well-defined absorption band at 360 nm with a narrow full width at half maximum of 66 nm (Fig. 2d) verified that both the size and the surface state of those sp^2 clusters contained in GQDs should be uniform, which may contribute to their strong fluorescence[42]. As the Nile Blue dye exhibits fluorescence maxima at ~675 nm upon 800 nm fs-laser excitation (Fig. S2), both the obtained GQD@Nile and GQD@Nile-E_2Zn_2SOD show well-resolved dual emission bands centered at ~465 and ~675 nm, respectively (Fig. 3 and Fig. S3). Using a femtosecond (fs) fluorescence measurement technique, the two-photon action cross section ($\Phi_F\sigma_{2P}$) of GQDs and Nile Blue at 800 nm were estimated to be 22.0 ± 6.0 GM and 1.6 ± 0.5 GM (Goeppert-Mayer unit), respectively.

The response of the dual-emission two-photon fluorescent probe to Cu^{2+} was then carried out to prove the working principle, as demonstrated in Fig. 3. Upon addition of Cu^{2+}, the blue emission from the GQDs shows continuous quenching, whereas the red emission from Nile Blue still remains constant. Furthermore, F_{blue}/F_{red}, the ratio of the integrated intensities at 450–600 nm (F_{blue}) and 620–700 nm (F_{red}), gradually decreases with the increasing concentration of Cu^{2+} and the signal ratio shows good linearity with Cu^{2+} concentration in the range of 2×10^{-7}–3×10^{-6} M. The detection limit was calculated to be ~100 nM (based on a signal-to-noise ratio of S/N = 3), which is comparable to those of previously reported Cu^{2+} biosensors[13–16]. The interaction between E_2Zn_2SOD and Cu^{2+} was further studied by optical spectroscopy (Fig. S4–S5) and XPS (Fig. S1). The absorption spectrum of the reconstituted SOD by Cu^{2+} was in a good agreement with that of native SOD with $\lambda_{max} = 680$ nm, but obviously different from that of a Cu^{2+} aqua ion and that of E_2Zn_2SOD. Meanwhile, two clear peaks ascribed to Cu_{2p} were observed at 932.74 and 952.74 eV in XPS obtained at the reconstituted SOD-modified surface, which were not obtained at the surfaces of bare GQDs, GQD@Nile, or GQD@Nile-E_2Zn_2SOD. In addition, for better understanding the quenching mechanism, the time-resolved fluorescence (TRF) signals of GQD@Nile-E_2Zn_2SOD were probed in the absence and presence of Cu^{2+} at 465 nm with an excitation at 400 nm (Fig. S6). In the absence of Cu^{2+}, the fluorescence decays single exponentially by 1.68 ns time constant, which is the lifetime of GQDs in the nanohybrids. However, the lifetime changed to 1.35 ns after Cu^{2+} was bond at the surface of GQDs by E_2Zn_2SOD, which may be explained for the fluorescence quenching by the excitation energy transfer from the GQDs to the copper d-orbital and/or GQDs to Cu^{2+} charge transfer[13,48]. The clear mechanism is unclear known at the present stage, because the fluorescence process of GQDs is still unclear and the related work is underway.

The complexity of intracellular system presents a great challenge for biosensors not only in sensitivity but more importantly in selectivity. The selectivity experiments were carried out by monitoring the intensity ratio (F_{blue}/F_{red}) of the probe in the presence of millimolar concentrations of Na$^+$, K$^+$, Ca^{2+}, and Mg^{2+}, 10 μM concentrations of Mn^{2+}, Fe^{2+}, Co^{2+}, Ni^{2+}, Zn^{2+}, and Cu$^+$, that may coexist in the living system. Remarkably, unperturbed fluorescence response (Fig. S7) was observed for the other metal ions, compared with that obtained for Cu^{2+}. Meanwhile, these potential metal ion interferences showed negligible effects on the signal for Cu^{2+} sensing. Taking into account that amino acids in the biological system are capable of interacting with a lot of metal cations, several typical amino acids were also examined. Little effect on the intensity ratios of the probes was obtained (Fig. S7) after their exposure to 10 μM concentrations of amino acids. On the other hand, an obvious decrease in the intensity ratio was observed upon the subsequent addition of 2 μM Cu^{2+}. In addition, negligible effect on the fluorescence probe was observed for the other biological species such as glutathione, glucose, hydrogen peroxide, proteins including cytochrome c, hemoglobin and myglobin (Fig. S7). Furthermore, the GQD@Nile-E_2Zn_2SOD signal was independent of solution pH in the biologically relevant pH (Fig. S8). The combined results reveal that GQD@Nile-E_2Zn_2SOD can detect Cu^{2+} with minimum interference from pH and from other metal ions, amino acids, and potential biological species due to the specific interaction of designed molecule E_2Zn_2SOD with Cu^{2+} to reconstitute SOD.

For biological application, the long-term cellular toxicity of GQD@Nile-E_2Zn_2SOD toward the A549 cell lines was determined by means of a standard MTT (methyl thiazolyl tetrazolium) assay[49,50]. In the presence of the GQD@Nile-E_2Zn_2SOD probe with the concentration from 20 to 1000 μg mL^{-1}, the cellular viabilities were estimated to be greater than 90% and 87% (Table S1) after incubation for 24 and 48 h, respectively. The results indicate that the GQDs-based probe is generally low-toxic for cellular imaging. The conclusion was also supported by the result of the flow cytometry experiments. Apoptosis assay confirmed no obvious increase of cell
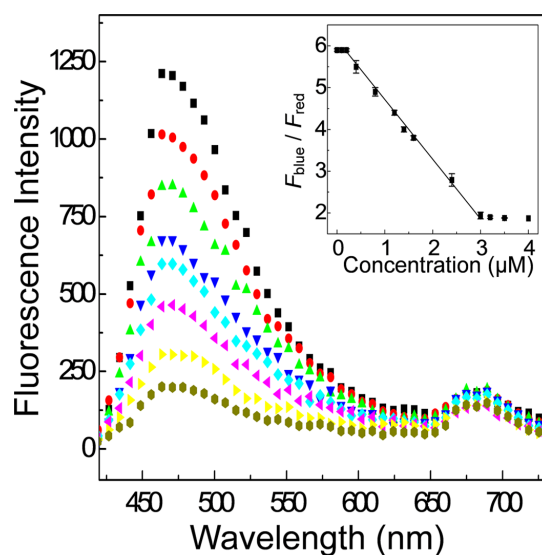

Figure 3 | Two-photon fluorescence spectra for the titration of GQD@Nile-E_2Zn_2SOD (0.1 mg mL^{-1}) with CuCl$_2$ (0–4 μM). Inset: plot of F_{blue}/F_{red} as a function of the Cu^{2+} concentration. Error bars represent standard error measurements (s.e.m.)

death or apoptosis after incubating cells with GQD@Nile-E_2Zn_2SOD (Fig. S9). Moreover, the two-photon excited fluorescence intensity of the GQD@Nile-E_2Zn_2SOD-labeled A549 cells remained nearly the same after continuous irradiation by the fs-pulses for 60 min, indicating its high photostability (Fig. S10).

We next sought to assess whether GQD@Nile-E_2Zn_2SOD as a two-photon probe could report changes in the Cu^{2+} level in live cells by ratiometric fluorescence imaging. Upon two-photon excitation at 800 nm, the emission ratio images of A549 cells labeled with GQD@Nile-E_2Zn_2SOD were constructed from two collection windows (Fig. S10, 450–600 nm, F_{blue} and 620–700 nm, F_{red}). From Fig. 4a, we can see that the average emission ratio is 5.56 ± 0.39, revealing very low levels of available Cu^{2+} in the normal condition. Then, GQD@Nile-E_2Zn_2SOD was responsive to the change in the Cu^{2+} concentration: the F_{blue}/F_{red} ratio decreased to 2.18 ± 0.51 when the cells were pre-incubated with 100 μM $CuCl_2$ (Fig. 4b). Treatment of cells with an excess of the cell-permeable, high affinity copper chelator, ethylene-diaminetetraacetic acid (EDTA), increases the fluorescence ratio to 4.77 ± 0.20 (Fig. 4c). These initial experiments in A549 cells demonstrate that we could observe changes in fluorescence ratios in cells treated with exogenous Cu sources. We then examined whether this indicator could be used to study the physiological process of intracellular binding of Cu^{2+} to E_2Zn_2SOD. In this context, L-ascorbic acid has been reported to inhibit the intracellular copper binding to apo-enzymes[51]. Fluorescence ratio images of A549 cells labeled with GQD@Nile-E_2Zn_2SOD revealed that L-ascorbic acid treatment depressed the reconstitution of E_2Zn_2SOD with Cu^{2+}, showing no obvious change in fluorescence ratio (the F_{blue}/F_{red} ratio only decreased to 4.20 ± 0.30) in cells when compared with solely Cu source treatment (Fig. 4b, d). More importantly, D-isoascorbic acid, the epimer of the ascorbic acid, had no effect on the change of fluorescence ratio in cells treated with exogenous Cu sources (the F_{blue}/F_{red} ratio decreased to 2.42 ± 0.35) (Fig. 4e). Clearly, the GQD@Nile-E_2Zn_2SOD probe provides a facile and effective model and strategy for evaluating the effects of L-ascorbic acid on intracellular Cu^{2+} binding to E_2Zn_2SOD.

To further investigate the utility of this probe in deep tissue imaging, TPM images were obtained from a part of lung cancer tissue slice incubated with 0.1 mg mL^{-1} GQD@Nile-E_2Zn_2SOD for 12 h at 278 K. As the structure of the obtained lung tissue slice is known to be inhomogeneous throughout its entire depth, we accumulated 10 TPM images from the two collection windows at depths of 90–180 μm to visualize the overall Cu^{2+} distribution. The concentrations of Cu^{2+} were estimated from the F_{blue}/F_{red} ratios and the titration curve (see above). Moreover, the image at a higher magnification clearly shows the Cu^{2+} distribution in the individual cells with an average emission ratio of 5.78 ± 0.56 at a depth of 120 μm (Fig. 5c). When the tissue was pretreated with 100 μM $CuCl_2$, the ratio decreased to 1.92 ± 0.48 (Fig. 5f). It is worth noting that the changes in the emission ratios measured deep inside the tissue are comparable to those in the cells. Furthermore, the TPM images at depths of 90, 120, 150, and 180 μm demonstrate that GQD@Nile-E_2Zn_2SOD is capable of detecting Cu^{2+} at depths of 90–180 μm in live tissues using TPM (Fig. S11).

Discussion

we have developed a new ratiometric two-photon probe, GQD@Nile-E_2Zn_2SOD, which shows a marked blue-to-yellow emission color change in response to Cu^{2+}, with high selectivity and accuracy. Meanwhile, the GDQ-based fluorescence probe demonstrates low cytotoxicity, insensitivity to pH over the biologically relevant pH range, long-term photostability, and good cell-permeability. As a consequence, the ratiometric probe can visualize Cu^{2+} levels in live cells and tissues at depths of 90–180 μm, and further evaluate the effect of L-ascorbic acid on intracellular Cu^{2+} binding to E_2Zn_2SOD. This work has opened up a way to understanding the role that Cu^{2+} plays in the biological and pathological systems, as well as provided a methodology to design organic-inorganic ratiometric two-photon probes for detection of metal ions and other biological species.
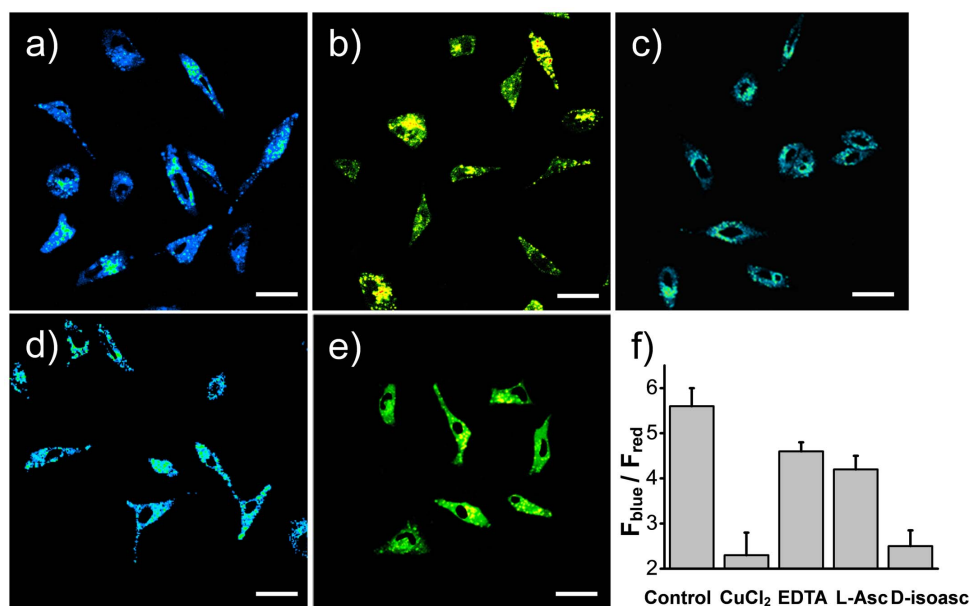

Figure 4 │ (a–e) Pseudocolored ratiometric TPM images (F_{blue}/F_{red}) of A549 cells. (a) The ratio images of live A549 cells grown in basal media and stained with GQD@Nile-E_2Zn_2SOD probes for 60 min at 37°C. (b) A549 cells pretreated with 100 μM $CuCl_2$ for 4 h and stained with fluorescent probes for 60 min at 37°C. (c) A549 cells pretreated with 100 μM $CuCl_2$ for 4 h and then EDTA for 30 min before stained with probes for 60 min at 37°C. (d) A549 cells incubated with 100 μM $CuCl_2$ for 4 h and then 1 mM L-ascorbic acid for 30 min before stained with probes for 60 min at 37°C. (e) A549 cells incubated with 100 μM $CuCl_2$ for 4 h and then 1 mM D-isoascorbic acid for 30 min before stained with probes for 60 min at 37°C. (f) Bar graph representing the integrated intensity from 450–600 nm over the integrated fluorescence intensity from 620–700 nm. Values are the mean ratios generated from the intensities from five randomly selected fields. Error bars represent standard error measurements (s.e.m.). Scale bar: 30 μm.
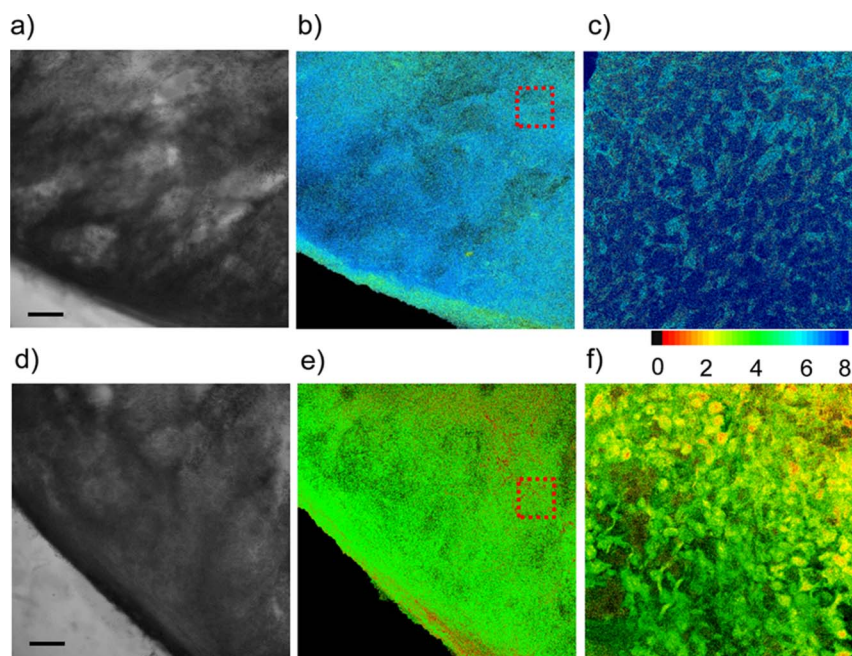
Figure 5 | Images of lung cancer tissue slice stained with GQD@Nile-E$_2$Zn$_2$SOD for 12 h. (a, d) Bright-field images of lung cancer tissue slices that were (a) not treat with and (d) pretreated with CuCl$_2$. (b, e) Ratiometric TPM images of lung cancer tissue slices that were (b) not treated with and (e) pretreated with CuCl$_2$. Ten ratiometric TPM images were accumulated along the z direction at depths of 90–180 μm with 10× magnification. (c, f) Enlarged images of the red boxes in (b) and (e) at a depth of 120 μm with 63× magnification. The TPEF was collected in two channels (blue = 450–600 nm, red = 620–700 nm) upon excitation at 800 nm with a pulse laser. Scale bars: 150 μm.

Methods

Synthesis of GQDs. Graphene quantum dots (GQDs) were synthesized following the method reported by Dong et al.[42]. Citric acid (2 g) was heated to 473 K until the color of the liquid was changed from colorless to orange in about 30 min. The orange liquid was then added to 100 mL of 10 mg mL^{-1} NaOH solution dropwise under vigorous stirring. The obtained graphene quantum dots solution was kept in refrigerator.

Preparation of E$_2$Zn$_2$SOD. The Cu-free derivative E$_2$Zn$_2$SOD was prepared according to the method described by Cocco[52]. Briefly, DDC was added to 0.1 mM SOD solutions, buffered with 0.1 M potassium phosphate at pH 7.4, at a final concentration of 0.5 mM. The mixture was incubated at 310 K for about 2 h until no further increase in absorbance at 450 nm was observed. Then, the yellow solution was centrifuged at 39000 g for 30 min, and the colorless supernatant was exhaustively dialysed against doubly distilled water. Finally, the E$_2$Zn$_2$SOD solution was lyophilized and kept in the refrigerator for further use.

Conjugation of GQD@Nile-E$_2$Zn$_2$SOD. For the synthesis of GQD@Nile-E$_2$Zn$_2$SOD, the obtained GQDs solution was mixed with Nile Blue chloride (10^{-4} M) and E$_2$Zn$_2$SOD (2×10^{-5} M) and stirred for 5 min. Then, EDC/NHS (20 mM) were added and stirred for ~2–4 h for the conjugation. Finally, the nanohybrids were separated from free EDC/NHS, unreacted Nile Blue chloride and E$_2$Zn$_2$SOD by three cycles of concentration/dilution (10 : 1), using a Nanosep centrifugal device (Pall Corporation, MW cutoff of 3 kDa), and redispersed in PBS buffer (pH = 7.4).

Linear optical properties. Linear absorption was measured with an Agilent 8453 UV-vis spectrophotometer. Fluorescence emission and excitation spectra were measured on a Hitachi F-2700 fluorescence spectrophotometer equipped with a 90 W Xenon lamp in a 1-cm cuvette. Fluorescence quantum yield (Φ) of GQDs was obtained from measurements at five different concentrations in HEPES buffer using the following equation:

$$\Phi_{FX} = \Phi_{FST} \left(\frac{Abs_{ST}}{Abs_X} \right) \left(\frac{\sum F_X}{\sum F_{ST}} \right) \left(\frac{\eta_X^2}{\eta_{ST}^2} \right) \qquad (1)$$

Where Φ_F is the quantum yield, Abs and F denote the absorbance and fluorescence intensity, respectively, and $\sum F$ denotes the peak area of the fluorescence spectra, calculated by summation of the fluorescence intensity. η is the refractive index of the solvent. ST is the standard and X is the sample. Quinine sulfate (literature $\Phi_F = 0.54$) was used as a standard[47], and excitation was performed at 400 nm.

Measurements of two-photon fluorescence excitation spectra and two-photon action cross section. The two-photon action cross section ($\Phi_F\sigma_{2P}$) was determined by using a femtosecond (fs) fluorescence measurement technique as described[53]. The two-photon excited fluorescence spectra were measured on a spectrometer (HORIBA Model iHR 550) and the pump laser beam came from a mode-locked Ti:sapphire laser (Coherent Mira 900) with a pulse duration of 80 fs and a repetition rate of 76 MHz. The two-photon excited fluorescence spectra of the reference and the sample were determined at the same excitation wavelength. Rhodamine B (0.6 μM) in MeOH was used as a reference, whose two-photon properties have been well characterized in the literature[54]. By taking the ratio of equation 2 for sample and reference, the two-photon action cross-section ($\Phi_F\sigma_{2P}$) of the sample was calculated.

$$F_{(t)} = \frac{1}{2} \eta C \Phi_F \sigma_{2P} g \frac{8n \langle P_{(t)} \rangle^2}{\pi \lambda} \qquad (2)$$

Here, $F_{(t)}$ = the time-averaged fluorescence photon flux, η = fluorescence collection efficiency, C = sample concentration, Φ_F = fluorescence quantum efficiency, σ_{2P} = non-linear two-photon absorption cross-section, g = degree of second order temporal coherence, n = index of refraction of medium lens works in, $P_{(t)}$ = instantaneous incident power, and λ = wavelength in vacuum.

Fluorescence lifetime measurement. Fluorescence lifetime measurements were performed on an Edinburgh Instruments (FLS 920) spectrometer by the time-correlated single photon counting (TCSPC) method. Excitation was achieved by a hydrogen-filled nanosecond flash lamp (repetition rate 40 kHz). Measurements were taken in ambient conditions, at room temperature, on solutions diluted to yield reasonable signal intensity. Excitation was performed at 400 nm for the GQD@Nile-E$_2$Zn$_2$SOD and the time-resolved emission data were collected at 465 nm. The TCSPC traces were analyzed by standard tail fit implemented in the software of the fluorimeter. Weighted residuals and χ^2 values were used to judge the quality of the fit.

Two-photon fluorescence microscopy. Two-photon fluorescence images of dye-labeled cells and tissues were obtained with spectral confocal and multiphoton microscopes (Leica TCS SP8) with ×10 dry and ×63 oil objectives, numerical aperture (NA) = 0.4 and 1.4. The two-photon fluorescence microscopy images were obtained with a DMI 6000 Microscope (Leica) by exciting the probes with a mode-locked titanium-sapphire laser source (Mai Tai DeepSee, 80 MHz, ~90 fs) set at wavelength 800 nm and output power 2920 mW. To obtain images at 450–600 nm (blue) and 620–700 nm (red) range, internal PMTs were used to collect the signals in an 8 bit unsigned 1024 × 1024 pixels at 200 Hz scan speed.

Cell culture and cytotoxicity assay. Human lung cancer cells line A549 were cultured in RPMI 1640 supplemented with 10% fetal bovine serum. When in the proliferative period, A549 cells (~3 × 10^5 cell mL^{-1}) were dispersed within replicate 96-well micro-liter plates to a total volume of 100 μL well^{-1} and maintained at 310 K in a 5% CO$_2$/95% air incubator for 24 h. Then, the culture media was removed and the cells were incubated in culture medium containing the as-prepared GQD@Nile-E$_2$Zn$_2$SOD with different concentrations for 24 h or 48 h and washed with the culture medium. An amount of 100 μL of the new culture medium containing MTT (10 μL,

5 mg mL^{-1}) was then added, followed by incubating for 4 h to allow the formation of formazan dye. After removing the medium, 150 μL DMSO was added to each well to dissolve the formazan crystals. Absorbance was measured at 490 nm in a Multiskan MK3 microplate photometer (Thermo Scientific). Cell viability values were determined (at least three times) according to the following formulae: cell viability (%) = mean of absorbance value of treatment group/mean absorbance value of control ×100%.

Flow cytometry. The percentage of apoptotic cells was determined by monitoring the translocation of phosphatidylserine to the cell surface using an Annexin V-FITC apoptosis detection kit (KeyGEN Biotech) according to the manufacturer's instructions. Briefly, after dye treatment, the cell culture medium was collected to retain floating cells and attached cells were dislodged using the EDTA-free trypsin. Floating and attached cells were combined and harvested by centrifugation. The cell pellets were suspended in 500 μL binding buffer and incubated with 5 μL FITC-Annexin V and 5 μL of a propidium iodide solution for 15 min in the dark. Cells were evaluated for apoptosis using a Becton-Dickinson flow cytometer with Annexin V–FITC and PI double staining. Fluorescence was measured with an excitation wavelength of 480 nm through FL-1 (530 nm) and FL-2 filters (585 nm).

Preparation and staining of lung cancer tissue slice. Tissue slices were prepared from A549 human lung cancer cells. A total of 2×10^6 A549 cells diluted in 200 μl of serum-free DMEM medium were injected subcutaneously into the right flank of 6- to 8-week-old BALB/c nude mice to inoculate tumors. On day 15 after A549 inoculation, mice were sacrificed. Tumors were removed and embedded with O.C.T (Sakura Finetek, USA, Torrance, CA) for frozen sections. The tissues were cut into 250 μm-thick slices using a vibrating-blade microtome. Slices were then treated with nanoprobe GQD@Nile-E$_2$Zn$_2$SOD for 12 h at 4°C. After washing with PBS, the slice were mounted with 10% glycerol and sealed with nail varnish on a glass substrate. The TPM images of lung cancer tissue labeled with nanoprobe were obtained at depths from 90 to 180 μm in a spectral confocal multiphoton microscope as shown in Figure S11.

1. Linder, M. C. & Hazegh-Azam, M. Copper biochemistry and molecular biology. *Am. J. Clin. Nutr.* **63**, 797S–811S (1996).
2. Que, E. L., Domaille, D. W. & Chang, C. J. Metals in neurobiology: probing their chemistry and biology with molecular imaging. *Chem. Rev.* **108**, 1517–1549 (2008).
3. Reddy, P. V. B., Rao, K. V. R. & Norenberg, M. D. The mitochondrial permeability transition, and oxidative and nitrosative stress in the mechanism of copper toxicity in cultured neurons and astrocytes. *Lab. Invest.* **88**, 816–830 (2008).
4. Valentine, J. S. & Hart, P. J. Misfolded CuZnSOD and amyotrophic lateral sclerosis. *Proc. Natl. Acad. Sci. U. S. A.* **100**, 3617–3622 (2003).
5. Davis, A. V. & O'Halloran, T. V. A place for thioether chemistry in cellular copper ion recognition and trafficking. *Nat. Chem. Biol.* **4**, 148–151 (2008).
6. Camakaris, J., Voskoboinik, I. & Mercer, J. F. Molecular mechanisms of copper homeostasis. *Biochem. Biophys. Res. Commun.* **261**, 225–232 (1999).
7. Barnham, K. J., Masters, C. L. & Bush, A. I. Neurodegenerative diseases and oxidative stress. *Nat. Rev. Drug Discov.* **3**, 205–214 (2004).
8. Zeng, L., Miller, E. W., Pralle, A., Isacoff, E. Y. & Chang, C. J. A selective turn-on fluorescent sensor for imaging copper in living cells. *J. Am. Chem. Soc.* **128**, 10–11 (2006).
9. Taki, M., Iyoshi, S., Ojida, A., Hamachi, I. & Yamamoto, Y. Development of highly sensitive fluorescent probes for detection of intracellular copper(I) in living systems. *J. Am. Chem. Soc.* **132**, 5938–5939 (2010).
10. Liu, J., Karpus, J., Wegner, S. V., Chen, P. R. & He, C. Genetically encoded copper(I) reporters with improved response for use in imaging. *J. Am. Chem. Soc.* **135**, 3144–3149 (2013).
11. Uauy, R., Olivares, M. & Gonzalez, M. Essentiality of copper in humans. *Am. J. Clin. Nutr.* **67**, 952S–959S (1998).
12. Kim, B. E., Nevitt, T. & Thiele, D. J. Mechanisms for copper acquisition, distribution and regulation. *Nat. Chem. Biol.* **4**, 176–185 (2008).
13. Jung, H. S. *et al.* Coumarin-derived Cu^{2+}-selective fluorescence sensor: synthesis, mechanisms, and applications in living cells. *J. Am. Chem. Soc.* **131**, 2008–2012 (2009).
14. Zhao, Y. *et al.* Highly sensitive and selective colorimetric and off-on fluorescent chemosensor for Cu^{2+} in aqueous solution and living cells. *Anal. Chem.* **81**, 7022–7030 (2009).
15. Lin, W., Long, L., Chen, B., Tan, W. & Gao, W. Fluorescence turn-on detection of Cu^{2+} in water samples and living cells based on the unprecedented copper-mediated dihydrorosamine oxidation reaction. *Chem. Commun.* **46**, 1311–1313 (2010).
16. Yu, M. *et al.* Highly sensitive and fast responsive fluorescence turn-on chemodosimeter for Cu^{2+} and its application in live cell imaging. *Chem. – Eur. J.* **14**, 6892–6900 (2008).
17. Qu, Q., Zhu, A., Shao, X., Shi, G. & Tian, Y. Development of a carbon quantum dots-based fluorescent Cu^{2+} probe suitable for living cell imaging. *Chem. Commun.* **48**, 5473–5475 (2012).
18. Zhu, A., Qu, Q., Shao, X., Kong, B. & Tian, Y. Carbon-dot-based dual-emission nanohybrid produces a ratiometric fluorescent sensor for in vivo imaging of cellular copper ions. *Angew. Chem.* **124**, 7297–7301 (2012).
19. Zhu, A., Qu, Q., Shao, X., Kong, B. & Tian, Y. Carbon-dot-based dual-emission nanohybrid produces a ratiometric fluorescent sensor for in vivo imaging of cellular copper ions. *Angew. Chem., Int. Ed.* **51**, 7185–7189 (2012).
20. Dong, Y. *et al.* Polyamine-functionalized carbon quantum dots as fluorescent probes for selective and sensitive detection of copper ions. *Anal. Chem.* **84**, 6220–6224 (2012).
21. Larson, D. R. *et al.* Water-soluble quantum dots for multiphoton fluorescence imaging in vivo. *Science* **300**, 1434 (2003).
22. Kim, H. M. & Cho, B. R. Two-photon probes for intracellular free metal ions, acidic vesicles, and lipid rafts in live tissues. *Acc. Chem. Res.* **42**, 863–872 (2009).
23. Pawlicki, M., Collins, H. A., Denning, R. G. & Anderson, H. L. Two-photon absorption and the design of two-photon dyes. *Angew. Chem., Int. Ed.* **48**, 3244–3266 (2009).
24. Terai, T. & Nagano, T. Fluorescent probes for bioimaging applications. *Curr. Opin. Chem. Biol.* **12**, 515–521 (2008).
25. He, G. S., Tan, L.-S., Zheng, Q. & Prasad, P. N. Multiphoton absorbing materials: molecular designs, characterizations, and applications. *Chem. Rev.* **108**, 1245–1330 (2008).
26. Sumalekshmy, S. & Fahrni, C. J. Metal-ion-responsive fluorescent probes for two-photon excitation microscopy. *Chem. Mater.* **23**, 483–500 (2010).
27. Kong, B. *et al.* Carbon dot-based inorganic-organic nanosystem for two-photon imaging and biosensing of pH variation in living cells and tissues. *Adv. Mater.* **24**, 5844–5848 (2012).
28. Morales, A. R. *et al.* Design, synthesis, and structural and spectroscopic studies of push-pull two-photon absorbing chromophores with acceptor groups of varying strength. *J. Org. Chem.* **78**, 1014–1025 (2013).
29. Liu, F. *et al.* Ratiometric detection of viscosity using a two-photon fluorescent sensor. *Chem. – Eur. J.* **19**, 1548–1553 (2013).
30. Jiang, Y. *et al.* Multibranched triarylamine end-capped triazines with aggregation-induced emission and large two-photon absorption cross-sections. *Chem. Commun.* **46**, 4689–4691 (2010).
31. Lee, J. H., Lim, C. S., Tian, Y. S., Han, J. H. & Cho, B. R. A two-photon fluorescent probe for thiols in live cells and tissues. *J. Am. Chem. Soc.* **132**, 1216–1217 (2010).
32. Zhu, M. Q. *et al.* Reversible two-photon photoswitching and two-photon imaging of immunofunctionalized nanoparticles targeted to cancer cells. *J. Am. Chem. Soc.* **133**, 365–372 (2010).
33. Lu, J., Yeo, P. S. E., Gan, C. K., Wu, P. & Loh, K. P. Transforming C60 molecules into graphene quantum dots. *Nat. Nanotech.* **6**, 247–252 (2011).
34. Liu, R., Wu, D., Feng, X. & Müllen, K. Bottom-up fabrication of photoluminescent graphene quantum dots with uniform morphology. *J. Am. Chem. Soc.* **133**, 15221–15223 (2011).
35. Shen, J., Zhu, Y., Yang, X. & Li, C. Graphene quantum dots: emergent nanolights for bioimaging, sensors, catalysis and photovoltaic devices. *Chem. Commun.* **48**, 3686–3699 (2012).
36. Pan, D., Zhang, J., Li, Z. & Wu, M. Hydrothermal route for cutting graphene sheets into blue-luminescent graphene quantum dots. *Adv. Mater.* **22**, 734–738 (2010).
37. Tachikawa, T., Cui, S.-C., Fujitsuka, M. & Majima, T. Interfacial electron transfer dynamics in dye-modified graphene oxide nanosheets studied by single-molecule fluorescence spectroscopy. *Phys. Chem. Chem. Phys.* **14**, 4244–4249 (2012).
38. Zhu, S. *et al.* Surface chemistry routes to modulate the photoluminescence of graphene quantum dots: from fluorescence mechanism to up-conversion bioimaging applications. *Adv. Funct. Mater.* **22**, 4732–4740 (2012).
39. Rotilio, G. *et al.* Properties of the apoprotein and role of copper and zinc in protein conformation and enzyme activity of bovine superoxide dismutase. *Biochemistry* **11**, 2182–2187 (1972).
40. Rigo, A. *et al.* The binding of copper ions to copper-free bovine superoxide dismutase. Properties of the protein recombined with increasing amounts of copper ions. *Biochem. J.* **161**, 31–35 (1977).
41. Yang, J.-I. *et al.* Detection of copper ions in liquid foods and beverages based on an enzymatic method. *J. Food Drug Anal.* **20**, 83–87 (2012).
42. Dong, Y. *et al.* Blue luminescent graphene quantum dots and graphene oxide prepared by tuning the carbonization degree of citric acid. *Carbon* **50**, 4738–4743 (2012).
43. Hontoria-Lucas, C., López-Peinado, A. J., López-González, J. d. D., Rojas-Cervantes, M. L. & Martín-Aranda, R. M. Study of oxygen-containing groups in a series of graphite oxides: physical and chemical characterization. *Carbon* **33**, 1585–1592 (1995).
44. Li, Y. *et al.* An electrochemical avenue to green-luminescent graphene quantum dots as potential electron-acceptors for photovoltaics. *Adv. Mater.* **23**, 776–780 (2011).
45. Peng, J. *et al.* Graphene quantum dots derived from carbon fibers. *Nano Lett.* **12**, 844–849 (2012).
46. Zhang, J. *et al.* Platelet adhesive resistance of segmented polyurethane film surface-grafted with vinyl benzyl sulfo monomer of ammonium zwitterions. *Biomaterials* **24**, 4223–4231 (2003).
47. Crosby, G. A. & Demas, J. N. Measurement of photoluminescence quantum yields. *J. Phys. Chem.* **75**, 991–1024 (1971).
48. Chakraborti, H., Sinha, S., Ghosh, S. & Pal, S. K. Interfacing water soluble nanomaterials with fluorescence chemosensing: graphene quantum dot to detect Hg^{2+} in 100% aqueous solution. *Mater. Lett.* **97**, 78–80 (2013).
49. You, Y. *et al.* Phosphorescent sensor for robust quantification of copper(II) ion. *J. Am. Chem. Soc.* **133**, 11488–11491 (2011).

50. Li, C. *et al.* A nonemissive iridium(III) complex that specifically lights-up the nuclei of living cells. *J. Am. Chem. Soc.* **133**, 11231–11239 (2011).

51. Harris, E. D. & Percival, S. S. A role for ascorbic acid in copper transport. *Am. J. Clin. Nutr.* **54**, 1193S–1197S (1991).

52. Misra, H. P. Reaction of copper-zinc superoxide dismutase with diethyldithiocarbamate. *J. Biol. Chem.* **254**, 11623–11628 (1979).

53. Xu, C. & Webb, W. W. Measurement of two-photon excitation cross sections of molecular fluorophores with data from 690 to 1050 nm. *J. Opt. Soc. Am. B* **13**, 481–491 (1996).

54. Makarov, N. S., Drobizhev, M. & Rebane, A. Two-photon absorption standards in the 550-1600 nm excitation wavelength range. *Opt. Express* **16**, 4029–4047 (2008).

Acknowledgments

Author contributions

Y.T. designed the research, analyzed the data and wrote the paper with assistance from A.Z. A.Z. performed the experiments and analyzed the data. C.D. performed the preparation of cell cultures and flow cytometry. All authors reviewed the manuscript.

Additional information

Supplementary information accompanies this paper at http://www.nature.com/scientificreports

Competing financial interests: The authors declare no competing financial interests.

How to cite this article: Zhu, A., Ding, C. & Tian, Y. A two-photon ratiometric fluorescence probe for Cupric Ions in Live Cells and Tissues. *Sci. Rep.* **3**, 2933; DOI:10.1038/srep02933 (2013).